Lab on a Chip

PAPER

Cite this: *Lab Chip*, 2025, **25**, 1823

Droplet microfluidic method for measurement of ultralow interfacial tension in ternary fluid systems†

Thai Dinh, Robert Casal and Thomas Cubaud *

Received 9th December 2024,
Accepted 24th February 2025

DOI: 10.1039/d4lc01047g

rsc.li/loc

We experimentally investigate droplet pattern formation in coaxial microchannels using ternary mixtures of two immiscible fluids and a miscible solvent. The influence of solvent concentration is examined through periodic pattern analysis of droplet flow and functional relationships are developed to determine the initial interfacial tension of dispersions made of aqueous mixtures of solvent and oil at short timescales, *i.e.*, when solvent diffusion into the continuous phase has a negligible effect on flow morphologies. We examine a wide range of flow rates and delineate vast flow maps of droplet regimes, including dripping and jetting flows, to clarify the hydrodynamic behavior of conjugate fluid mixtures in square microcapillaries. A method based on analysis of droplet size and spacing is implemented to predict the role of the miscible fluid additive concentration in microfluidic multiphase flows of water–isopropanol and ethanol–isopropanol blends in viscous silicone oil. This approach enables measurement of extremely small values of interfacial tension at large solvent concentrations. This work shows a technique for exploring and characterizing numerous ternary flow systems of interest with a variety of organic solvents and oils.

Introduction

Liquid–liquid dispersions are an important class of materials that find use in a range of applications, including in the food,[1,2] cosmetics,[3] medical,[4,5] and pharmaceutical industries,[6,7] as well as during oil recovery.[8,9] The stability of emulsions revolves around numerous factors, including fluid physicochemical properties, flow parameters, and the presence of surface active agents to lower interfacial tension and stabilize droplets against coalescence.[10–12] While thermodynamic equilibria between two liquid phases depend on chemical affinity and consist of ideal solutions for miscible fluids and separate layers or dispersions for immiscible fluids, the situation of partially miscible fluids and systems made of three components presents more complex aspects as the solubility of ternary fluid systems also depends on fluid concentration.[13] In particular, the phase behavior of ternary fluid systems made of two immiscible phases, such as water and oil, and a miscible solvent, is typically represented using Gibbs triangular diagrams where binodal and spinodal curves delineate the various states of the mixture, including regions of spontaneous emulsification, which is sometimes referred to as the "ouzo effect", where fine dispersions naturally form as a result of the interplay of solvent exchange and interfacial tension phenomena. By contrast to surfactant molecules, which typically lower interfacial tension up to the critical micelle concentration, miscible solvents can reduce interfacial tension over multiple orders of magnitude, which presents significant advantages for the elaboration of novel functional materials. However, whereas the thermodynamic stability of ternary mixtures has been extensively studied at long timescales,[14–16] less is known about their microflow behavior at short timescales.[17–19] Therefore, it would be useful to clarify the evolution of ternary fluid systems using microflow contactors and develop methods for the measurement of the initial interfacial tension of mixtures made of immiscible fluids with miscible additives at short time scales. In turn, better understanding of time-evolving droplet microfluidic flows is important for the improvement of solvent extraction methods for enhancing separation and purification techniques, including during water treatment and the recycling of oils.

Microfluidic devices provide unique platforms for the manipulation of liquid–liquid multiphase flows in confined microgeometries with precise control over flow rates and injection configurations.[20–24] Monodisperse trains of droplets are routinely produced in straight, rectangular microchannels using a variety of fluid contactors, including T-junction,[25–29] hydrodynamic and flow-focusing sections,[30–35] as well as coaxial microfluidic channels.[36–38] The centerline injection of coaxial devices is useful for the fabrication of microfibers[39,40] as well as other applications, such as high-pressure microreactors[41] and

Department of Mechanical Engineering, Stony Brook University, Stony Brook, NY 11794, USA. E-mail: thomas.cubaud@stonybrook.edu

† Electronic supplementary information (ESI) available. See DOI: https://doi.org/10.1039/d4lc01047g

high-throughput cell sorters.[42] Coaxial microcapillaries also offer the possibility to produce small droplets in the absence of wetting of the dispersed phase with the walls, which in turn facilitates systematic interrogation of the role of fluid properties in dispersed flows of immiscible and miscible fluids.[43] A variety of microfluidic methods were previously developed to measure dynamic interfacial tension, including through deformation and retraction of drops under extensional flow,[26] pressure drop measurements,[44] drop size,[45] and analysis of jetting/dripping transitions.[22] While ultralow values of interfacial tension, *i.e.*, below 1 mN m^{-1}, were measured and confirmed with a spinning drop apparatus using the jetting/dripping transition method, techniques based on regime transitions are limited to the external selection of flow rates and the visual distinction of flow regimes, which is challenging for small droplet sizes. Hence, a method based on the continuous evolution of droplet flow patterns would be useful to measure extremely low values of interfacial tension and shed light on out-of-equilibrium fluid processes with ternary fluid systems, including spontaneous emulsification and droplet dissolution phenomena, in microfluidic devices.

Here, we employ coaxial microdevices to examine segmented flows with ternary fluids in the situation where droplets are made of a mixture of a polar phase and a solvent in a continuous phase of oil. We demonstrate that solvent diffusion into the external phase is negligible at the short timescales of our microflow experiments and we devise a functional method based on periodic droplet pattern analysis for the measurement of dynamic interfacial tension between the mixture and the oil as a function of solvent concentration. We conduct systematic experiments covering a wide range of flow rates and solvent concentrations for two types of ternary fluid systems, including water–isopropanol and ethanol–isopropanol mixtures in silicone oil. This approach is selected to examine a large span of interfacial tension, from moderate values for pure fluids to ultralow values at large additive concentrations. We discuss the evolution of flow maps and regime transition between typical dispersed flow patterns, including the dripping and jetting regimes, as well as for separated flows with the stable jet regime. Basic features of dilute arrays of small droplets are modelled to analyze the influence of flow velocity on the morphological evolution of flow patterns at various solvent concentrations. In particular, the decrease of the spacing between droplets is examined at fixed volume fractions and functional relationships are developed to quantitatively predict the correspondence between flow rates and solvent concentration. The multiphase flow characteristics of the pure fluid pairs are used as a foundation to study the behavior of the ternary fluid pairs and droplet pattern analysis is employed to determine extremely small interfacial tension in complex multiphase systems at the small scale.

Materials and methods

We investigate the behavior of microfluidic droplets made of a mixture of aqueous fluid and solvent in oil using coaxial microchannels. The miniature flow device consists of an assembly of a square glass microcapillary of width h = 500 μm in which a cylindrical microneedle, having an outer diameter d_O = 305 μm and inner diameter d_I = 152 μm, is centrally inserted. The microneedle is composed of stainless steel with a blunt flat tip and used to inject the dispersed phase (fluid L1) at flow rate Q_1 into the main channel where the continuous phase (fluid L2) is flowing along the channel axis at flow rate Q_2. The microfluidic device is mounted into a custom-made frame where two cameras (X-PRI AOS Technology and PL-B771U Pixelink) equipped with 50 mm macro lenses and extension tubes are positioned to visualize fluid motion at a resolution of about 3 μm per pixel at variable frame rate ranging from a few to 4000 frames per second in both planes parallel to the flow. A micro-stage is attached to the device outlet to precisely align the microneedle along the microchannel centerline using the two cameras. Fluids are injected into the device using syringe pumps (New Era Pump Systems, Inc. NE-1010) and gas-tight syringes (Hamilton) with a volume of 1 ml for the dispersed phase and 2.5 ml for the continuous phase to finely control volumetric flow rates ranging between 4×10^{-2} and 1×10^{2} μL min^{-1}.

The solvent used is isopropyl alcohol, which is referred to as IPA (ACS reagent, ≥99.5%), and two types of aqueous mixtures are investigated, including blends of absolute ethanol (200 proof, ACS reagent, ≥99.5%) and IPA as well as mixtures of DI water and IPA for the droplet phase L1. The volumetric solvent concentration in the mixture is calculated according to $\Phi_S = V_S/(V_A + V_S)$, where V_S is the solvent volume and V_A the volume of the aqueous phase, *i.e.*, either water or ethanol. Fluids are mixed at room temperature with a stirrer at 1200 rpm for about an hour before each experiment and Φ_S is varied between 0 and 1. The continuous phase L2 is made of conventional silicone oil (polydimethylsiloxane), having a kinematic viscosity of 100 cSt (Gelest DMS-T21). Basic fluid properties of pure components are shown in Table 1. The interfacial tension γ_0 of pure fluid pairs with silicone oil, *i.e.*, DI water in oil and ethanol in oil, is measured using a Du Nouy ring tensiometer and corresponds to 42.7 mN m^{-1} and 0.75 mN m^{-1}, respectively. Previous work has shown that the fluid pair, isopropanol and 100 cSt silicone oil, is miscible,[46] therefore the effective interfacial tension γ_i of a given mixture at concentration $\Phi_S = i$ with the oil is expected to range between γ_0 for $\Phi_S = 0$ and $\gamma_1 = 0$ mN m^{-1} for $\Phi_S = 1$. Hence, the large difference in γ_0 between water and ethanol enables exploring multiphase flows over a

Table 1 Fluid properties of pure fluids, including density ρ and dynamic viscosity η

Fluid	ρ (g ml^{-1})	η (cP)
DI water	1.000	0.90
Ethanol	0.789	1.07
Isopropanol	0.785	2.10
PDMS oil	0.966	96.6

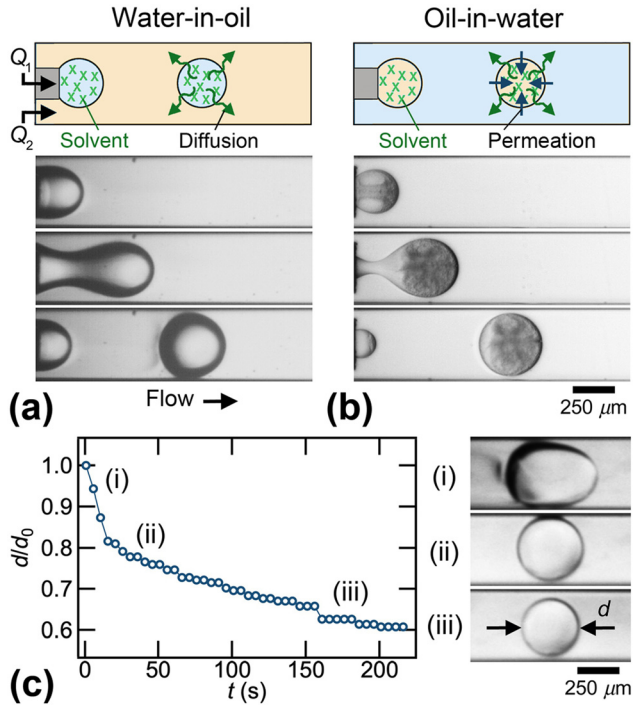

Fig. 1 Behavior of droplets infused with solvent in coaxial microchannels. (a) Time-series of ethanol–isopropanol droplet formation in oil at $\Phi_S = 0.3$ with schematics showing outward solvent diffusion, flow rates $Q_1 = 0.1$ and $Q_2 = 2$ μl min^{-1}. (b) Time-series of oil–isopropanol droplet formation in ethanol at $\Phi_S = 0.3$ with schematics showing outward solvent diffusion and inward polar phase permeation leading to spontaneous emulsification, flow rates $Q_1 = 0.5$ and $Q_2 = 25$ μl min^{-1}. (c) Temporal evolution of a water–isopropanol droplet in oil at $\Phi_S = 0.99$ showing significant decrease in droplet size d at long times. (i)–(iii) Corresponding time-series of droplet evolution in the reference frame of the droplet.

large range of interfacial tension with focus on ultra-low values, which are obtained at large solvent concentrations Φ_S, while maintaining a nearly constant mixture viscosity $\eta_1 \sim 10^0$ cP and density ρ_1.

Our experimental approach enables systematic investigations of ternary fluid system behavior in microchannels. For example, two complementary situations are displayed in Fig. 1(a) and (b) for solvent-infused droplets using the same fluids but different preparation steps. When the solvent is mixed with the polar phase, regular arrays of droplets are formed for the water-in-oil type, and spontaneous emulsification of droplets is observed for solvent–oil mixtures in the oil-in-water case. As the solvent is miscible in the two phases, outward diffusion fluxes are expected in both cases, however, the strong affinity of solvent and aqueous fluids in the oil-in-water case leads to the inward permeation of the polar phase into droplets to recombine with the solvent. Hence, a range complex solutal fluxes and Marangoni flows develop near microfluidic contactors, *i.e.*, at the tip of microneedles in coaxial channels, and further insight is required to better understand the evolution of ternary fluid properties as a function of solvent concentration in microchannels.

In this work, we focus on the water-in-oil type and show that diffusive effects are limited over the range of flow rates investigated, which enables measurement of instantaneous interfacial tension at short time scales. By contrast, at long time scales, solvent-infused droplets progressively dissolve in oil as shown in Fig. 1(c) for the case of an experiment where the flow was stopped. It is found, in particular, that the droplet sharply decreases in size in the first few seconds and slowly deflates over minutes. Therefore, the diffusive nature of solvent necessitates the development of original microfluidic methods for the measurement of interfacial tension in ternary fluid systems. In the following, we examine the influence of Φ_S on dilute droplet microfluidic flows made of the fluid mixture L1 in a continuous phase of silicone oil L2 at small viscosity ratio $\chi = \eta_1/\eta_2 \sim 10^{-2}$ at short time scales $\tau < 1$ s, *i.e.*, immediately after droplets formed at the microneedle tip. Dilute droplet regimes are obtained at low flow volume fractions $\alpha_1 = Q_1/(Q_1 + Q_2) < 0.5$, which correspond to small flow rate ratios $\varphi = Q_1/Q_2 < 1$. A method of analysis consists in examining the evolution of dispersed flows at fixed φ – to set the droplet flow concentration α_1 – as a function of the average flow velocity $J = Q_T/h^2$, where the total flow rate $Q_T = Q_1 + Q_2$. This approach facilitates the formulation of functional relationships based on φ and Q_T to further characterize the role of fluid properties in microfluidic droplet flow characteristics.

Flow maps

A systematic series of experiments is conducted to examine droplet microflow patterns with water–IPA and ethanol–IPA mixtures for Φ_S ranging between 0 and 1. By varying the total flow rate $Q_T = Q_1 + Q_2$ across multiple flow rate ratios $\varphi = Q_1/Q_2$, we observe familiar dispersed flow patterns such as dripping and jetting, as well as separated flows, including various core-annular flows, such as stable, wavy, and wetting jet regimes, as shown in Fig. 2 for the case of ethanol-based mixtures. For a given flow rate ratio $\varphi \leq 1$, the droplet forms at the fluid contactor in the dripping regime at low total flow rates Q_T and is emitted from the tip of the central stream in the jetting regime at moderate Q_T. At larger flow velocities, the central stream adopts the shape of a stable jet of constant width ε in the field of view $x/h \sim 10$. Other regimes, such as wavy and wetting jets, are found at relatively large values of $\varphi \sim 1$ and are beyond the scope of this study.

Flow maps presented in the form of φ plotted against Q_T show regime classification depending on total flow rates. A progressive shift in flow transitions, such as for the dripping–jetting and jetting–stable jet transitions, is observed toward lower values of Q_T as Φ_S increases [Fig. 2(a)]. In particular, at low $\Phi_S = 0.2$, only dispersed flows (dripping and jetting) are visible in the range of Q_T varying from 10^{-1} to 10^2 μL min^{-1} while at high $\Phi_S = 0.8$, core-annular flows occupy most of the flow map. Overall, as the solvent concentration increases between fluid pairs, morphological transformations of regular droplet arrays are observed in the microchannel with a decrease of droplet size d and spacing L at larger Φ_S, as can be seen in the droplet flow chart at $\varphi = 3 \times 10^{-2}$ displayed in Fig. 2(b). Representation in the (Φ_S, Q_T)-

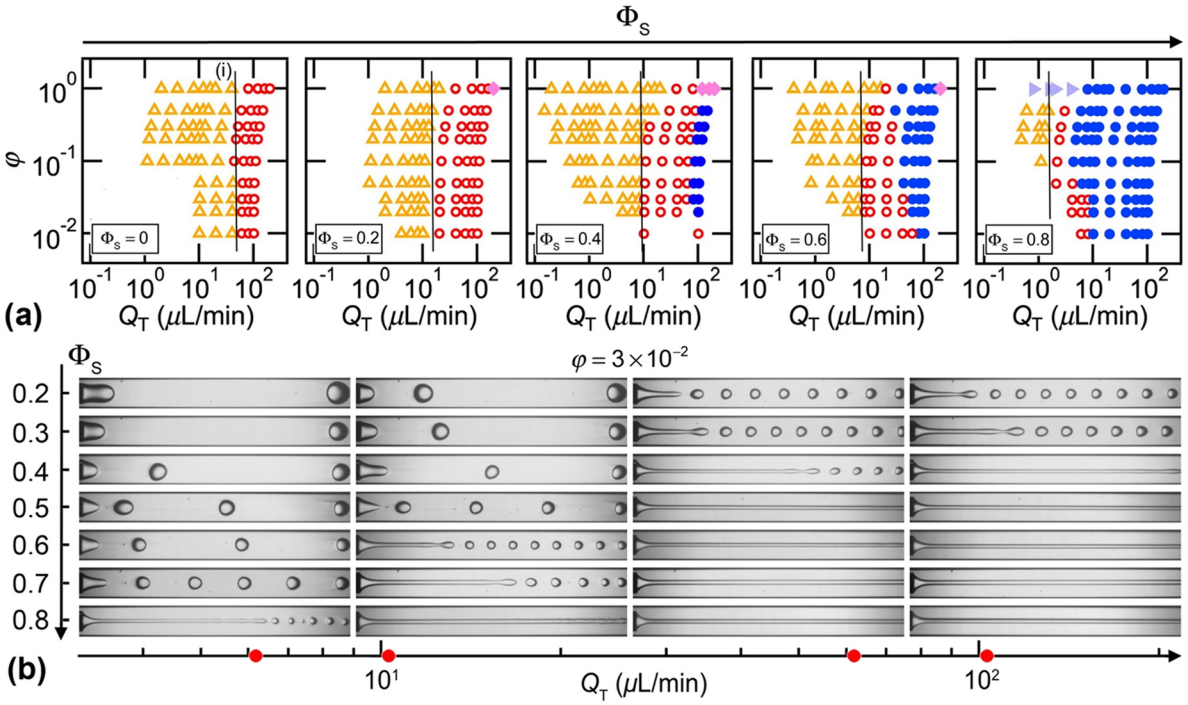

Fig. 2 (a) Flow maps of ethanol–IPA mixtures in 100 cSt silicone oil at five solvent concentrations Φ_S = 0, 0.2, 0.4, 0.6, and 0.8 in the (φ, Q_T) parameter plane. Symbols: dripping (△), jetting (○), stable jet (●), wavy jet (◆), wetting jet (►). Line (i): dripping–jetting transition at low φ. (b) Flow chart with micrographs of ethanol–IPA mixtures at fixed flow rate ratio $\varphi = 3 \times 10^{-2}$ for Φ_S ranging from 0.2 to 0.8 at different total flow rates Q_T = 6.18, 10.3, 61.8, and 103 μL min^{-1}.

parameter space at fixed φ highlights the combined influence of solvent concentration and flow velocity on periodic droplet patterns, where droplet arrays obtained at large Φ_S and small Q_T (bottom left corner on the chart) present strong similarities with those obtained at small Φ_S and large Q_T (upper right corner). Hence, we propose a methodological approach based on periodic analysis of flow patterns at small viscosity ratio $\chi \sim 10^{-2}$ to elucidate the relationship between (a) flow parameters, such as φ and Q_T, and (b) fluid properties, such as interfacial tension γ and solvent concentration Φ_S. In this work, we ultimately relate γ and Φ_S based on the reference interfacial tension γ_0 of pure fluid pairs and demonstrate a technique to measure ultralow γ at large Φ_S.

Dilute droplet regime

Coaxial microfluidic devices provide means for the generation of regular arrays of small droplets at low φ. Here, we focus on two main characteristics of droplet microflows, including the droplet size d and spacing L, in the dilute regime $\varphi \leq 1$ to investigate the influence of solvent concentration Φ_S. In this case, droplets remain small in size $d/h \leq 1$ and, as observed with side cameras, retain a nearly spherical geometrical shape, which facilitates modelling of droplet flow characteristics based on control parameters Q_1 and Q_2. For constant $\varphi = Q_1/Q_2$, the change in droplet size d/h with $Q_T = Q_1 + Q_2$ is relatively negligible while the droplet spacing L/h experiences a significant decrease as illustrated in Fig. 3(a). Assuming negligible solvent exchange between fluids and conservation of mass per unit cell of the

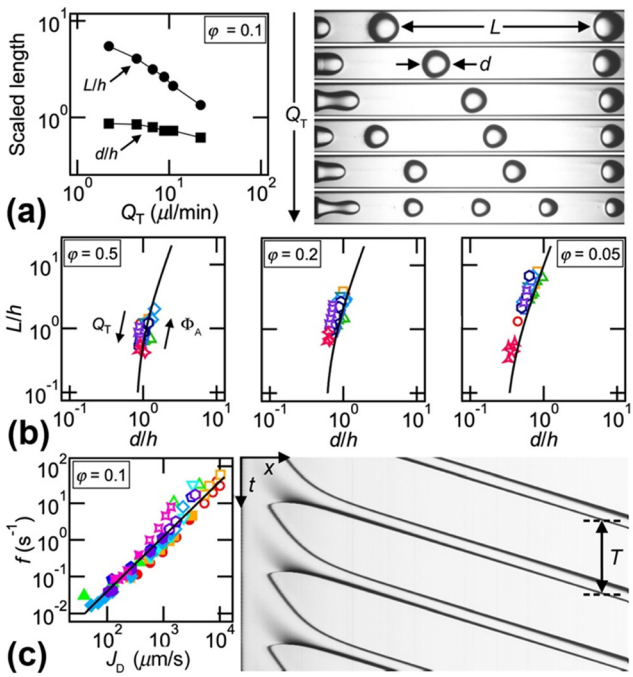

Fig. 3 (a) Left: Evolution of droplet size d/h and spacing L/h as a function of Q_T at φ = 0.1 for ethanol–IPA mixtures at Φ_S = 0.1. Right: Corresponding micrographs with flow rates in μL min^{-1} and (Q_1, Q_2) = (0.2, 2), (0.4, 4), (0.6, 6), (0.8, 8), (1, 10), and (2, 20) from top to bottom. (b) Droplet spacing L/h *versus* droplet size d/h at φ = 0.5, 0.2, 0.05 for all Φ_S with ethanol–IPA mixtures. See text for solid lines. (c) Left: Emission frequency f *versus* droplet velocity J_D in dripping and jetting regimes at φ = 0.1 for all Φ_S with ethanol–IPA and water–IPA mixtures. Solid line: $f = 4 \times 10^{-5}\ J_D^{1.5}$. Right: Example of a spatiotemporal diagram of droplet formation showing measurement of emission period T.

segmented flow of length $\lambda = d + L$ over a period of droplet emission T, the droplet volume V_1 reads $Q_1T = (\pi/6)d^3$ and the continuous phase volume V_2 is modeled as $Q_2T = (d + L)h^2 - (\pi/6)d^3$. Hence, for a given $\varphi = Q_1/Q_2$, the droplet size and spacing are related to φ such as $\varphi^{-1} = [(d + L)h^2]/[(\pi/6)d^3] - 1$. Then, along an iso-$\varphi$ curve, the spacing L/h depends on d/h according to $L/h = (\varphi^{-1} + 1)(\pi/6)(d/h)^3 - d/h$. We plot measurements of L/h for various fluid pairs, *i.e.*, at different Φ_S, *versus* d/h and find that data collapse along curves defined by theory [Fig. 3(b)]. Small deviation is observed at very low flow rate ratio φ as at high Q_T, droplets slightly depart from a spherical shape and exhibit a blunt back and pointy front. Overall, each iso-φ curve defines a family of periodic multiphase flows with low L at high Q_T and larger spacing at high aqueous volume fraction Φ_A, with $\Phi_S + \Phi_A = 1$ as displayed in Fig. 3(b). This finding confirms that the initial mass transfer between fluids is negligible over the relatively short residence times of droplets in the field of view near the fluid contactor, which suggests that the role of solvent concentration Φ_S is essentially limited to a reduction of initial interfacial tension γ between ternary fluid systems.

To further examine the behavior of regular droplet flow patterns, the droplet emission frequency f is also measured in dispersed flows, including dripping and jetting, and compared with the droplet velocity J_D [Fig. 3(c)-left]. An example of spatiotemporal diagram generated to measure the droplet emission period $T = 1/f$ and velocity J_D is shown in Fig. 3(c)-right. The straight lines corresponding to the droplet trajectories in the diagram show, in particular, that J_D does not change over time, as expected for non-diffusive systems. A simple model of droplet pattern assumes that the emission frequency f scales with droplet velocity J_D according to $J_D = \lambda f$. For $\varphi = 10^{-1}$, data for f fall into a single curve and follow a scaling law for all fluid pairs according to $f \sim J_D^{1.5}$. Deviation from basic modeling is expected as the wavelength $\lambda = d + L$ is not constant at fixed φ [Fig. 3(a)]. The collapse of data points into a master curve shows, nonetheless, the regularity of droplet emission frequency of ternary fluid systems across multiple time scales, which supports previous findings of negligible impact of solvent exchange between dispersed and continuous phases over the range of parameters investigated. Hence, periodic analysis of droplet patterns offers a means to characterize the influence of solvent concentration Φ_S on the initial interfacial properties of ternary fluid mixtures.

Detailed analysis of the evolution of droplet spacing L/h for the reference case of pure ethanol in oil at low φ reveals the relatively simple role of the total flow rate in flow patterns, according to $L/h \sim cQ_T^{-1/3}$, where c depends on φ, as shown in Fig. 4(a). We employ the method of iso-φ curves to determine the relationship between c and φ, and find that the constant c is well fit with the function of the form $c = c_0\varphi^{-1}$, where $c_0 = 0.75$ (μl min^{-1})$^{1/3}$ [Fig. 4(b)-inset]. Hence, the droplet spacing L/h is expected to scale inversely as $\varphi Q_T^{1/3}$, which enables collapsing data onto a master curve defined as $L/h = k_0(\varphi Q_T^{1/3})^{-1}$ where the constant $k_0 = 2.11 \times 10^{-4}$ m s$^{-1/3}$ for pure ethanol and oil multiphase flows, *i.e.*, at $\Phi_S = 0$ [Fig. 4(b)]. We generalize this method to analyze multiphase flows made of droplets having

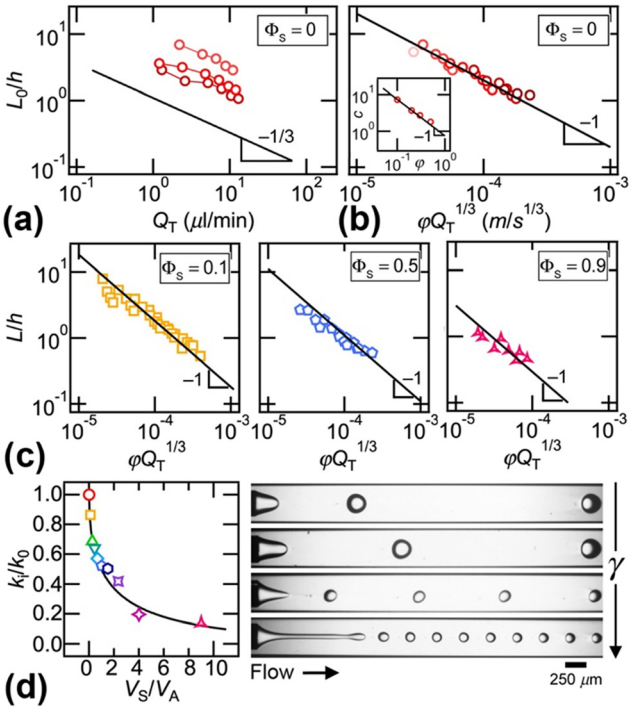

Fig. 4 (a) Droplet spacing L/h of pure ethanol in oil *versus* total flow rate Q_T of varied flow rate ratios φ = 0.1, 0.2, and 0.3. (b) L/h of Φ_S = 1.0 *versus* scaled parameters $\varphi Q_T^{1/3}$. Inset: Prefactor c *versus* φ. (c) L/h *versus* $\varphi Q_T^{1/3}$ of Φ_S = 0.1, 0.5, 0.9. (d) Factor ratio k_i/k_0 of all fluid pairs for ethanol–IPA mixtures in oil. Solid line: $k_i/k_0 = \exp[-0.7(V_S/V_A)^{1/2}]$. Micrographs of Φ_S = 0, 0.2, 0.4, and 0.8 from top to bottom at (Q_1, Q_2) = (0.4, 20).

various solvent concentrations Φ_S in the same oil and find that L/h follows a similar scaling law, such as $L/h = k_i(\varphi Q_T^{1/3})^{-1}$, where k_i is the prefactor obtained from curve-fitting L/h *versus* $(\varphi Q_T^{1/3})^{-1}$, which significantly decreases with Φ_S as can be seen in Fig. 4(c). Finally, we are looking for a simple functional relationship between k_i and Φ_S, however, since the solvent concentration $\Phi_S = V_S/(V_S + V_A)$ is bounded between 0 and 1, we plot instead the relative dimensionless change in prefactor k_i/k_0 as a function of the volume ratio of solvent within droplets $V_S/V_A = \Phi_S/(1 - \Phi_S)$, which varies between zero and infinity, and find good fit with an exponential decay formula, such as $k_i/k_0 = \exp[-0.7(V_S/V_A)^{1/2}]$ for ethanol–IPA mixtures [Fig. 4(d)]. A similar expression is found for water–IPA mixtures according to $k_i/k_0 = \exp[-0.4(V_S/V_A)^{1/4}]$ as seen in Fig. 5(a)-inset. Incidentally, using the solvent volume ratio V_S/V_A in functional analysis enables exploring very large solvent concentration Φ_S up to 99% for water–IPA mixtures. Overall, as interfacial tension is expected to reduce with Φ_S, the inner phase forms minute droplet size with smaller spacing as shown in micrographs displayed in Fig. 4(d)-right.

Measurement of instantaneous interfacial tension

Multiphase flows of immiscible fluids in coaxial microchannels at low viscosity ratio $\chi \sim 10^{-2}$ and various interfacial tensions γ were previously shown to follow the general relationship $L/h =$

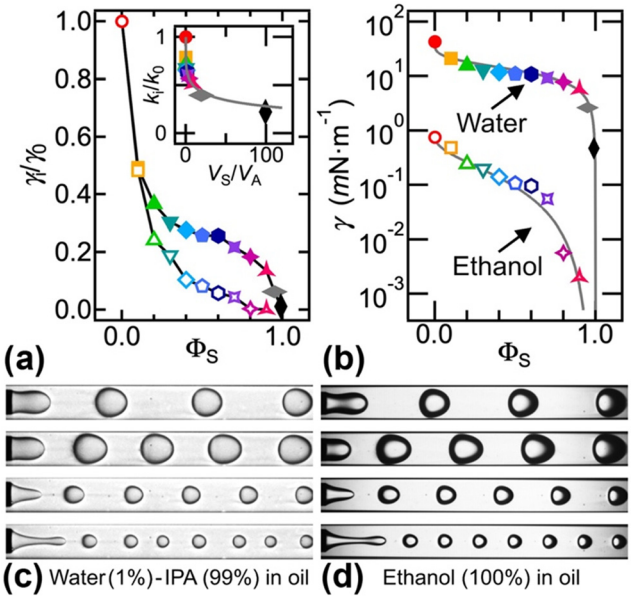

Fig. 5 Comparison of water–IPA (solid symbols) and ethanol–IPA (open symbols) mixtures in 100 cSt-silicone oil. Flow rates in μL min^{-1}. (a) Evolution of relative initial interfacial tension γ_i/γ_0 as a function of solvent concentration Φ_S. Inset: Prefactor ratio k_i/k_0 for water–IPA mixture *vs.* solvent volume ratio V_S/V_A. Solid line: $V_S/V_A = \exp(-0.4\Phi_S^{1/4})$. (b) Measurement of initial interfacial tension γ at various Φ_S. Solid lines: water–IPA mixture, $\gamma = 42.7(\exp\{-0.4[\Phi_S/(1-\Phi_S)]^{1/4}\})^3$; ethanol–IPA mixtures, $\gamma = 0.75(\exp\{-0.7[\Phi_S/(1-\Phi_S)]^{1/2}\})^3$. (c) Micrographs of water–IPA in oil ($\Phi_S = 0.99$): from top to bottom (Q_1, Q_2) = (0.3, 1), (0.5, 1), (0.6, 6), and (0.4, 8). (d) Micrographs of ethanol in oil ($\Phi_S = 0$): from top to bottom (Q_1, Q_2) = (1.8, 6), (3, 6), (4, 40), and (3, 60).

$C(\varphi Ca_T^{1/3})^{-1}$, where $Ca_T = \eta_2 Q_T/(\gamma h^2)$ is the capillary number of each fluid pair and C is a constant.[43] Here, the scaling $L_i/h = k_i(\varphi Q_T^{1/3})^{-1}$ is expressed in terms of capillary number such as $L_i/h = k_i(\eta_2/\gamma_i h^2)^{1/3}(\varphi Ca_T^{1/3})^{-1}$, where γ_i is the interfacial tension of fluid pair L1/L2 at concentration $\Phi_S = i$. Hence, it follows that the constant $C = k_i(\eta_2/\gamma_i h^2)^{1/3} = k_0(\eta_2/\gamma_0 h^2)^{1/3}$, which shows $k_i/k_0 = (\gamma_i/\gamma_0)^{1/3}$ since the oil continuous phase remains constant $\eta_2 = 96.6$ cP as well as channel size $h = 500$ μm. This approach shows that the relative shift in interfacial tension γ_i/γ_0 is related to the shift in prefactor according to $\gamma_i/\gamma_0 = (k_i/k_0)^3$. In other words, the change in interfacial tension γ_i is compensated for with total flow rate Q_T as the solvent concentration varies. Using this method, we plot the evolution of γ_i/γ_0 as a function of Φ_S for both water–IPA and ethanol–IPA mixtures in Fig. 5(a). While a similar behavior is observed at low IPA concentration with a two-fold decrease in γ_i/γ_0 for $\Phi_S = 0.1$, values for water-based mixtures remain higher than those for ethanol-based mixtures due to specific intermolecular interaction between these fluids. Previous studies on modeling and predicting interfacial tension of ternary mixtures[47–49] showed that for systems with the same solvent, interfacial tension may vary differently as presently observed.

This simple technique enables direct measurement of interfacial tension γ_i of ternary fluid at various Φ_S based on interfacial tension of pure fluid γ_0 at $\Phi_S = 0$, as shown in Fig. 5(b). In this work, a wide range of interfacial tension measurements with larger values are obtained for water–IPA mixtures in oil, from $\gamma_0 = 42.7$ mN m^{-1} at $\Phi_S = 0$ to $\gamma = 0.47$ mN m^{-1} at $\Phi_S = 0.99$, and ultralow values are measured for ethanol–IPA mixtures in oil from $\gamma_0 = 0.75$ mN m^{-1} at $\Phi_S = 0$ to $\gamma = 0.002$ mN m^{-1} at $\Phi_S = 0.9$. For a given fluid pair, interfacial tension is found to decrease by about two orders of magnitude from low to large Φ_S. Function relationships developed for the evolution of k_i/k_0 as a function of V_S/V_A and transposed for predicting γ_i as a function of Φ_S, *i.e.*, $\gamma_i = \gamma_0(\exp\{-a[\Phi_S/(1-\Phi_S)]^b\})^3$, with constants a and b depending on specific fluid intermolecular interactions. These curves show good agreement with interfacial tension data as indicated with gray curves in Fig. 5(b). We also find similarity in flow morphology of the water–IPA mixture with $\Phi_S = 0.99$ [Fig. 5(c)] and pure ethanol in oil [Fig. 5(d)], $\Phi_S = 0$, at different flow rates. To achieve the same flow patterns in pure ethanol in oil, the total flow rate Q_T used in the water–IPA ($\Phi_S = 0.99$) mixture is about six times smaller than that of the pure ethanol in oil case. Finally, to validate our microfluidic method for measurement of interfacial tension γ, we also conduct experiments with droplets made of water and ethanol mixtures in a continuous phase of silicone oil as shown in the ESI.† In this case, water–ethanol mixtures are immiscible with the oil, which permits measurements of interfacial tension γ using the traditional method of Du Nouy ring tensiometry and good agreement is found between the two techniques. Owing to the various curve fittings, assumptions, and operating conditions required to determine interfacial tension, the uncertainty in the method is estimated to about 20% of the measured value of γ, as discussed in the ESI.† Hence, our approach is particularly effective at measuring ultralow values of γ in the case of diffusive ternary fluid systems at large Péclet numbers while typical methods such as the Du Nouy ring and the spinning drop methods are preferable for non-diffusive systems due to their lack of fine control of the contact time between fluids. Overall, the proposed method shows a wide range of interfacial tension determination, from large to extremely small values using a rather simple analytical method based on the unique properties of microflows.

Conclusion

In this work, we demonstrate a method based on analysis of droplet microfluidic regimes to determine the initial interfacial tension of ternary fluid systems with viscous oils. Specifically, we examine the evolution of flow maps based on flow rate ratio φ and total flow rate Q_T as a function of solvent concentration of the aqueous droplet phase Φ_S and highlight the combined effect of flow velocity and solvent concentration on the characteristics of periodic dispersed flows. In the diluted regime, droplets adopt a nearly spherical shape, which facilitates geometrical modeling of droplet arrangements into regular patterns with negligible mass transfer. At short time scales, the droplet size d/h does not change significantly compared to the spacing L/h. Therefore,

we utilize an iso-φ curve approach to compare the evolution of L/h based on Q_T and Φ_S and develop functional relationships to predict the role of solvent concentration on microfluidic multiphase flows of water–isopropanol and ethanol–isopropanol mixtures in viscous silicone oil. Then, we develop a technique to estimate the relative interfacial tension of ternary fluids γ_i/γ_0 based on the relative shift in flow properties k_i/k_0 at various solvent concentrations Φ_S. We find that the interfacial tension γ_i of fluid mixtures with low original interfacial tension γ_0 decreases drastically with Φ_S compared to that of strongly hydrophilic fluid combinations with high γ_0.

Overall, this technique is promising for exploring and characterizing numerous ternary flow systems of interest with a variety of organic solvents and oils. Examining complementary injection schemes, including water-in-oil and oil-in-water multiphase flows, as well as oil–solvent mixtures to initiate spontaneous emulsification would clarify the intriguing behavior of ternary fluid systems in microflow reactors at short time scales. The reduction of test fluid volume needed for microfluidic characterization also makes the method appealing for investigating out-of-equilibrium thermodynamic paths of ternary fluids in the presence of surfactant to stabilize fluid structures formed during solvent exchange and synthesize advanced soft materials. Further work on the evolution of flow patterns at longer time scales would also shed light on the transport properties of partially miscible fluids in porous-like media.

Data availability

The data supporting this article have been included as part of the ESI.†

Conflicts of interest

The authors declare no competing financial interest.

Acknowledgements

This material is based upon work supported by the National Science Foundation under Grand No. CBET-2223988.

References

1 A. C. Karaca, N. Low and M. Nickerson, *Food Res. Int.*, 2011, **44**, 2742.
2 J. Maldonado-Valderrama, P. Wilde, A. Macierzanka and A. Mackie, *Adv. Colloid Interface Sci.*, 2011, **165**, 36.
3 V. K. Morya, C. Ahn, S. Jeon and E. K. Kim, *Mini-Rev. Med. Chem.*, 2013, **13**, 1761.
4 K. Ferrara, R. Pollard and M. Borden, *Annu. Rev. Biomed. Eng.*, 2007, **9**, 415.
5 S. Deshpande, Y. Caspi, A. E. C. Meijering and C. Dekker, *Nat. Commun.*, 2016, 7.
6 D. O. Grigoriev, T. Bukreeva, H. Möhwald and D. G. Shchukin, *Langmuir*, 2008, **24**, 999.
7 B. Brime, M. A. Moreno, G. Frutos, M. P. Ballesteros and P. Frutos, *J. Pharm. Sci.*, 2002, **91**, 1178.
8 N. R. Morrow and G. Mason, *Curr. Opin. Colloid Interface Sci.*, 2001, **6**, 321.
9 D. N. Espinoza and J. C. Santamarina, *Water Resour. Res.*, 2010, **46**, W07537.
10 F. Leal-Calderon, V. Schmitt and J. Bibette, *Emulsion Science: Basic Principles*, Springer, New York, 2007.
11 C. N. Baroud, F. Gallaire and R. Dangla, *Lab Chip*, 2010, **10**, 2032.
12 S. Jakiela, S. Makulska, P. M. Korczyk and P. Garstecki, *Lab Chip*, 2011, **11**, 3603.
13 G. W. Castellan, *Physical Chemistry*, Addison-Wesley Publishing Company, Reading, Massachusetts, 1983.
14 N. Shahidzadeh, D. Bonn, J. Meunier, M. Nabavi, M. Airiau and M. Morvan, *Langmuir*, 2000, **16**, 9703.
15 S. A. Vitale and J. L. Katz, *Langmuir*, 2003, **19**, 4105.
16 C. Solans, D. Morales and M. Homs, *Curr. Opin. Colloid Interface Sci.*, 2016, **22**, 88.
17 R. Hajian and S. Hardt, *Microfluid. Nanofluid.*, 2015, **19**, 1281.
18 M. F. Haase and J. Brujic, *Angew. Chem., Int. Ed.*, 2014, **53**, 11793.
19 L. Nan, H. Zhang, D. A. Weitz and H. C. Shum, *Lab Chip*, 2024, **24**, 1135.
20 B. Morin, Y. Liu, V. Alvarado and J. Oakey, *Lab Chip*, 2016, **16**, 3074.
21 T. Krebs, K. Schroen and R. Boom, *Lab Chip*, 2012, **12**, 1060.
22 M. Moiré, Y. Peysson, B. Herzhaft, N. Pannacci, F. Gallaire, L. Augello, C. Dalmazzone and A. Colin, *Langmuir*, 2017, **33**, 2531.
23 I. Bihi, D. Vesperini, B. Kaoui and A. Le Goff, *Phys. Fluids*, 2019, **31**, 062001.
24 H. M. Xia, J. W. Wu, J. J. Zheng, J. Zhang and Z. P. Wang, *Lab Chip*, 2021, **21**, 1241.
25 M. De Menech, *Phys. Rev. E*, 2006, **73**, 031505.
26 J. T. Cabral and S. D. Hudson, *Lab Chip*, 2006, **6**, 427.
27 W. H. Tan and S. Takeuchi, *Adv. Mater.*, 2007, **19**, 2696.
28 S. M. S. Murshed, S. H. Tan and N. T. Nguyen, *J. Phys. D: Appl. Phys.*, 2008, **41**, 085502.
29 M. De Menech, P. Garstecki, F. Jousse and H. A. Stone, *J. Fluid Mech.*, 2008, **595**, 141.
30 A. M. Gañán-Calvo and J. M. Gordillo, *Phys. Rev. Lett.*, 2001, **87**, 274501.
31 S. L. Anna, N. Bontoux and H. A. Stone, *Appl. Phys. Lett.*, 2003, **82**, 364.
32 P. Garstecki, I. Gitlin, W. DiLuzio, G. M. Whitesides, E. Kumacheva and H. A. Stone, *Appl. Phys. Lett.*, 2004, **85**, 2649.
33 N. Pannacci, H. Bruus, D. Bartolo, I. Etchart, T. Lockhart, Y. Hennequin, H. Willaime and P. Tabeling, *Phys. Rev. Lett.*, 2008, **101**, 189901.
34 W. Lee, L. M. Walker and S. L. Anna, *Phys. Fluids*, 2009, **21**, 032103.
35 X. Hu and T. Cubaud, *J. Fluid Mech.*, 2020, **887**, A27.
36 I. G. Loscertales, A. Barrero, I. Guerrero, R. Cortijo, M. Marquez and A. M. Gañán-Calvo, *Science*, 2002, **295**, 1695.

37 O. A. Basaran, *AIChE J.*, 2002, **48**, 1842.
38 P. Guillot, A. Colin, A. S. Utada and A. Ajdari, *Phys. Rev. Lett.*, 2007, **99**, 104502.
39 H. Onoe, *et al.*, *Nat. Mater.*, 2013, **12**, 584.
40 Y. R. Yu, F. F. Fu, L. R. Shang, Y. Cheng, Z. Z. Gu and Y. J. Zhao, *Adv. Mater.*, 2017, **29**, 1605765.
41 P. J. A. Sazio, *et al.*, *Science*, 2006, **311**, 1583.
42 A. Wolff, I. R. Perch-Nielsen, U. D. Larsen, P. Friis, G. Goranovic, C. R. Poulsen, J. P. Kutter and P. Telleman, *Lab Chip*, 2003, **3**, 22.
43 T. Dinh and T. Cubaud, *Langmuir*, 2021, **37**, 7420.
44 X. Wang, A. Riaud, K. Wang and G. Luo, *Microfluid. Nanofluid.*, 2015, **18**, 503.
45 K. Wang, Y. C. Lu, J. H. Xu and G. S. Luo, *Langmuir*, 2009, **25**, 2153.
46 T. Cubaud, B. Conry, X. Hu and T. Dinh, *Phys. Rev. Fluids*, 2021, **6**, 094202.
47 H. C. Kim and D. J. Burgess, *J. Colloid Interface Sci.*, 2001, **241**, 509.
48 A. Erfani, S. Khosharay and C. P. Aichele, *J. Chem. Thermodyn.*, 2019, **135**, 241.
49 A. Hernández, *Int. J. Thermophys.*, 2020, **41**, 125.